







# Signature of Extended Solar Cycles as Detected from Ca II K Synoptic Maps of Kodaikanal and Mount Wilson Observatory

Subhamoy Chatterjee<sup>1</sup> , Dipankar Banerjee<sup>1,2</sup> , Scott W. McIntosh<sup>3</sup> , Robert J. Leamon<sup>4</sup>, Mausumi Dikpati<sup>3</sup> ,  
Abhishek K. Srivastava<sup>5</sup>, and Luca Bertello<sup>6</sup>

<sup>1</sup> Indian Institute of Astrophysics, Koramangala, Bangalore 560034, India; [dipu@iiap.res.in](mailto:dipu@iiap.res.in)

<sup>2</sup> Center of Excellence in Space Sciences India, IISER Kolkata, Mohanpur 741246, West Bengal, India

<sup>3</sup> High Altitude Observatory, National Center for Atmospheric Research, P.O. Box 3000, Boulder, CO 80307, USA

<sup>4</sup> Department of Astronomy, University of Maryland College Park, MD 20742, USA

<sup>5</sup> Department of Physics, Indian Institute of Technology (BHU), Varanasi-221005, India

<sup>6</sup> National Solar Observatory, 3665 Discovery Drive, Boulder, CO 80303, USA

Received 2019 February 16; revised 2019 March 8; accepted 2019 March 8; published 2019 March 20

## Abstract

In recent years there has been a resurgence of the study of extended solar cycles (ESCs) through observational proxies mainly in extreme ultraviolet. But most of them are limited only to the space-based era covering only about two solar cycles. Long-term historical data sets are worth examining for the consistency of ESCs. The Kodaikanal Solar Observatory (KSO) and the Mount Wilson Observatory (MWO) are two major sources of long-term Ca II K digitized spectroheliograms covering the temporal spans of 1907–2007 and 1915–1985 respectively. In this study, we detected supergranule boundaries, commonly known as networks, using the Carrington maps from both KSO and MWO data sets. Subsequently we excluded the plage areas to consider only the quiet Sun (QS) and detected small-scale bright features through intensity thresholding over the QS network. Latitudinal density of those features, which we named “Network Bright Elements,” could clearly depict the existence of overlapping cycles with equatorward branches starting at latitude  $\approx 55^\circ$  and taking about  $15 \pm 1$  yr to reach the equator. We performed a superposed epoch analysis to depict the similarity of those extended cycles. Knowledge of such equatorward band interaction, for several cycles, may provide critical constraints on solar dynamo models.

*Key words:* methods: data analysis – Sun: chromosphere – Sun: faculae, plages – techniques: image processing

## 1. Introduction

Solar cycles are representatives of periodic variation of solar magnetic activity. Different features such as sunspots and plages observed in different wavelength bands serve as potential proxies for representing the solar magnetic cycle. The latitudinal locations of such features when plotted against time produce the well-known “Butterfly diagram.” The most prominent patterns in a Butterfly diagram, i.e., equatorward branches repeat over a timescale of 11 yr on average. These patterns generated from sunspot and plages depict negligible temporal overlap between two subsequent cycles. But the scenario changes when one starts observing the smaller-scale magnetic features. Several studies in the past have presented observations of small-scale features such as ephemeral regions (Wilson et al. 1988; Tlatov et al. 2010) and coronal bright points (McIntosh et al. 2014) to depict a temporal overlap of subsequent equatorward branches lasting more than half a decade and named them “extended solar cycles (ESCs).” Apart from those small-scale features, a signature of ESCs was observed by Altrock (1997) from latitudinal distribution of coronal green line (Fe XIV) emission. This study was later substantiated by Tappin & Altrock (2013) with more data corresponding to different coronal heights. They also pointed out that the onset of high latitude activity coincides with current cycle maxima. Another study by Juckett (1998) presented evidence for a 17 yr solar cycle in coronal hole topology and interplanetary magnetic field directions at 1 au. However, there are arguments that ESCs seen from coronal emissions are merely poleward concentrations of trailing polarity flux of the old cycle and not the precursors of a new solar cycle (Robbrecht et al. 2010). Signatures of ESCs were also found

from residual solar differential rotation, i.e., torsional oscillation or latitudinal migration of subsurface zonal flow bands (Labonte & Howard 1982; Snodgrass & Wilson 1987; Howe 2009). Thus, observation of ESCs across a wide range of heights indicates an obvious connection with the sunspot cycle. However, the evolution of ESCs to the sunspot butterfly diagram is something that has not been studied well with the dynamo theory. This study requires linking of different scales of features and may well provide some missing links to the dynamo models. A detailed study on ESCs may therefore allow us to constrain the solar cycle predictions (Tlatov 2007) and to better estimate their impact on space climate. ESCs, having temporal overlap of two active latitude bands, can play a critical role in substantiating the solar cycle impact on latitudinal origins of CMEs (Song et al. 2007; McIntosh et al. 2015). Uniform historical data in such a case can be extremely useful to know the consistency of such temporal overlaps between two cycles. Several observatories such as Kodaikanal, Mount Wilson, Meudon, Arcetri, etc., archived chromospheric data for several cycles before the space era. Successful ESC observations through EUV bright points (McIntosh et al. 2014) inspired us to look at the small-scale brightening in Ca II K networks as deep rooting of EUV bright points could possibly indicate the connection with Ca II K networks. Among all observatories, the Kodaikanal Solar Observatory (KSO) and the Mount Wilson Observatory (MWO), archived the longest time span of Ca II K images in digitized form. We used those two data sets in this study.

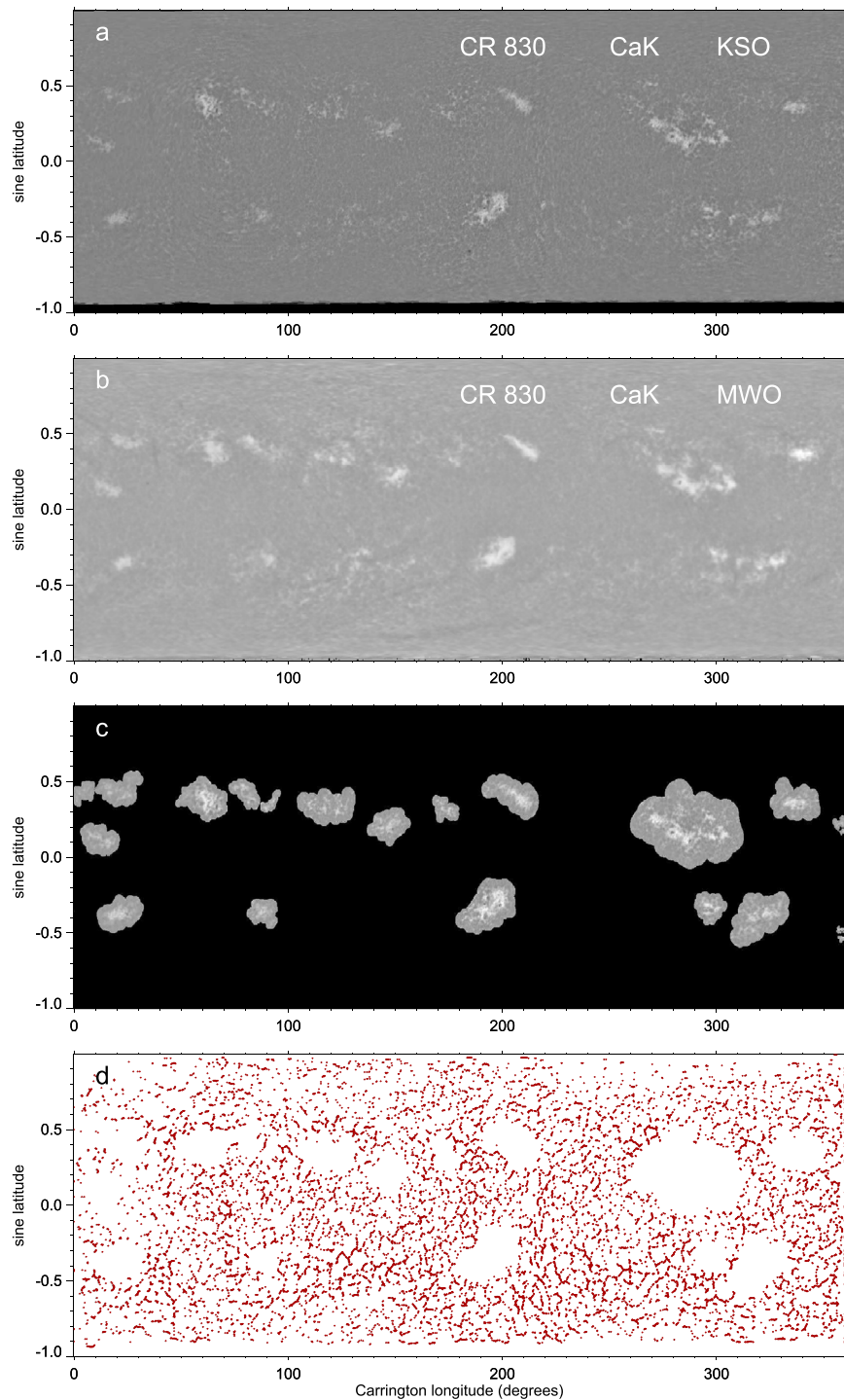


**Figure 1.** Observational Data and detection of network bright elements (NBEs) from Carrington maps. (a) Representative Carrington map for rotation 830 generated from Kodaikanal (KSO) Ca II K full-disk images. (b) Same Carrington rotation in Ca II K from Mt. Wilson Observatory (MWO). (c) Plage areas for rotation 830 masked with some margin outside depending on the size of plage to segregate the QS for NBE detection. (d) Binary map of detected NBEs (red symbols) by thresholding over networks. Please note that symbol size has been chosen for visual representation of NBE locations and is not an accurate representation of the area covered by NBE.

## 2. Observational Data Description

Full-disk Ca II K spectroheliograms (1907–2007) observed by KSO have recently been digitized and calibrated. Chatterjee et al. (2016) have generated Carrington maps of  $1571 \text{ pixels} \times 500 \text{ pixels}$  in Carrington longitude versus  $\sin(\text{latitude})$  grid (Figure 1(a)) using the calibrated data. A total of 1184 (between rotation number 716 and 2000) KSO carrington maps

have been used in this study. To find consistency of our detection and to improve the statistics we also used a total of 928 (from rotation 827 to 1763) MWO Ca II K Carrington maps (Figure 1(b)) between the years 1915 and 1985 (Sheeley et al. 2011).

The previous study by Chatterjee et al. (2016) from KSO showed clear degradation of plage area cycle after the year 1990. This is attributed to the poor data quality and data gaps,

resulting in low density of data points (see Figure 1 of Chatterjee et al. 2016). As bright regions on networks are much-smaller-scale features compared to plages, it is likely that data artifacts will affect them more. Similarly, Priyal et al. (2014) also restricted their detection of polar network elements from KSO Ca II K data until cycle 21. Furthermore, since we have detected the network elements from Carrington maps, discontinuity of data affects detection significantly. For these reasons, we have restricted our analysis from KSO data until 1990, i.e., the Carrington rotation 1837 (starting on 1990 December 19).

### 3. Analysis of Data

In the following subsections we describe the steps of the data analysis and the corresponding results.

#### 3.1. Detection of Quiet Sun (QS) Network Bright Elements (NBEs)

Networks manifest as bright polygonal structures in the Ca II K images circumscribing the supergranules. The supergranules have been detected from Kodaikanal images by Chatterjee et al. (2017) through watershed transform (McIntosh et al. 2011). The watershed transform sees the grayscale image as a topographic surface with height as intensities. The surface consists of hills and valleys. Watershed transform, also known as the “basin finding algorithm,” detects the local minimas of the surfaces and fills the valleys unless neighboring ones start overlapping. Consequently, all the supergranular structures are detected separated by networks. We have used the same technique to detect the networks of the Carrington maps. After extracting the networks, the active regions/plages were blocked with bigger masks. Plages were detected from the Carrington maps using the method described in Chatterjee et al. (2016). For creating the masks, the plage binary maps were dilated by a circular Kernel having size proportional to the size of the plages (Figure 1(c)). This was done to avoid any effect of active regions on bright element detection. After blocking the plages, an intensity threshold of (median+0.5 $\sigma$ ) was applied on the QS network to extract the brightenings, which we named “NBEs” (Figure 1(d)). The median and standard deviation( $\sigma$ ) were calculated over the QS network intensities.

#### 3.2. Time–Latitude Diagram of NBE Density

For generating the time–latitude diagram, first each Carrington map was divided into 36 latitude strips each 5° wide. Then, for  $i$ th strip the QS NBE density ( $d_i$ ) was calculated using latitudinal area covered by NBEs ( $A_i$ ), QS area ( $Q_i$ ), and data gap ( $G_i$ ) as  $d_i = \frac{A_i}{Q_i - G_i}$ . This step provided the latitudinal density of QS NBEs as a 36 element vector for each Carrington map. These vectors stacked over all the rotations resulted in the time–latitude map of NBE densities. Before deriving the final map, we smoothed every latitude bin over time with a kernel 200 rotations wide and divided the original map with a smoothed map to equalize the contrast across latitudes. The final maps generated from KSO and MWO data are shown in Figures 2(a) and (b) both clearly depicting extended equatorward branches having substantial temporal overlap with previous and next. The consistency of ESC detection from KSO and MWO is depicted in Figure 2(c). It shows that the KSO extended equatorward branch for cycle 20 is completed

when the gap in KSO NBE time–latitude is filled with MWO NBE density of overlapping times.

#### 3.3. “Terminators” and Extended Equatorward Branches

We defined “Terminators” as the epochs where the extended cycles come to an end meeting the solar equator (McIntosh et al. 2019). Before detecting “Terminators,” we smoothed different latitudes of Figures 2(b) and (c) with kernel of width 60 rotations to generate the plots shown in Figures 3(a) and (b). We fitted a third degree polynomial to the smoothed NBE density at the equator within a time span of  $[T_{\text{init}} - 4, T_{\text{init}} + 4]$  yr having the form  $\text{NBE} = p_0 + p_1T + p_2T^2 + p_3T^3$ . Here,  $T_{\text{init}}$  defines the initial guess about Terminators. We defined the final values of Terminators as the points of inflection of fitted polynomials (Table 1) mathematically defined as  $T = -p_2/3p_3$ . Using the  $1\sigma$  uncertainties ( $\Delta p_2, \Delta p_3$ ) of the polynomial coefficients from fitting we calculated the uncertainties in terminator locations as  $\Delta T = \sqrt{(1/3p_3)^2\Delta p_2^2 + (p_2/3p_3^2)^2\Delta p_3^2}$ . The smoothed plots (Figures 3(a) and (b)), especially the one from MWO, clearly depict the bifurcation into a poleward branch and an equatorward branch at  $\approx \pm 55^\circ$  latitude consistent with the study by McIntosh et al. (2014, 2019).

Thus to deduce the time duration of extended equatorward branches, we also determined the epochs at which those start ( $S$ ) at  $\pm 55^\circ$  latitude and uncertainties ( $\Delta S$ ) in those for north and south separately using the same method as that used for determining “Terminators.” By connecting those start epochs at  $\pm 55^\circ$  and the “Terminators” at equator, we found the fits for equatorward branches (Figures 3(a) and (b)). The duration of equatorward branches for different cycles, presented in Table 1, were calculated as  $D = T - S$ . The uncertainties in the cycle duration ( $\Delta D$ ) were derived using quadrature sum of start epoch uncertainty and terminator uncertainties, i.e.,  $\Delta D^2 = \Delta S^2 + \Delta T^2$ . It can be observed from both Figures 3(a) and (b) that equatorward branches of cycle-19 and cycle-20 had the least temporal overlap. Also MWO data shows smaller asymmetry between north and south equatorward branches with more uniform error bars for all cycles as compared to those for KSO (Table 1). We find good agreement between “Terminators” determined from KSO and MWO (Table 1, Figure 3).

#### 3.4. Similarity of Overlapping Cycles: “Superposed Epoch Analysis”

Superposed Epoch Analysis (SEA) is used to reveal periodicity in a data series through evaluation of statistical moments and also helps to recover signal from noise (Chree 1913). As the name suggests, this method works by superposition of several epochs of equal length selected about a reference time called “key time.” To select the basis for SEA in our study we selected “Terminators” as the “key times.” Epochs were selected as the time–latitude distributions within the interval [Terminator–11 yr, Terminator+11 yr]. Five such consecutive epochs were selected starting from cycle-15 Terminator for KSO and four consecutive epochs were selected for MWO starting from cycle-16 Terminator. Subsequently, the epochs were averaged to depict the mean epoch (Figures 4(a) and (c)). Mean epoch for both KSO and MWO clearly depicted the significant temporal overlap of successive equatorward branches confirming the consistency of ESCs over several

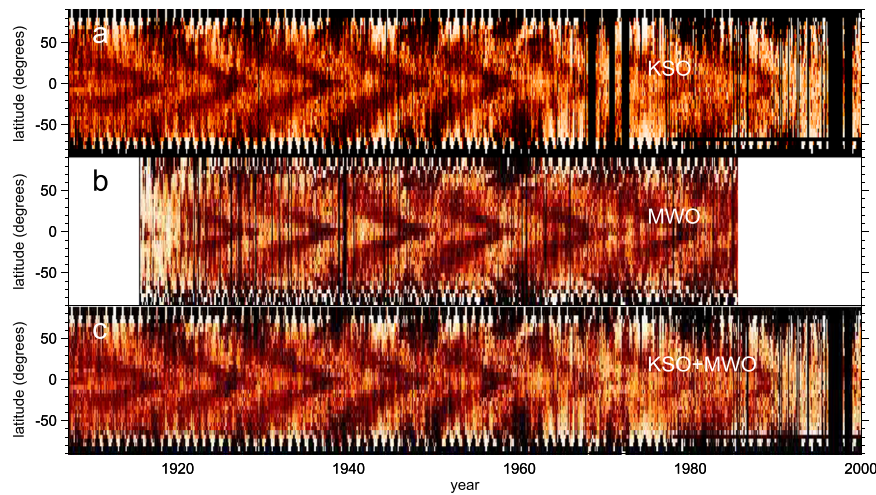


**Figure 2.** NBE time–latitude distribution. (a) Time–latitude plot of NBE density from KSO data. (b) Time–latitude plot of NBE density generated from MWO data. (c) Time–latitude plot of NBE density from KSO with data gaps after 1960 filled with MWO time–latitude.

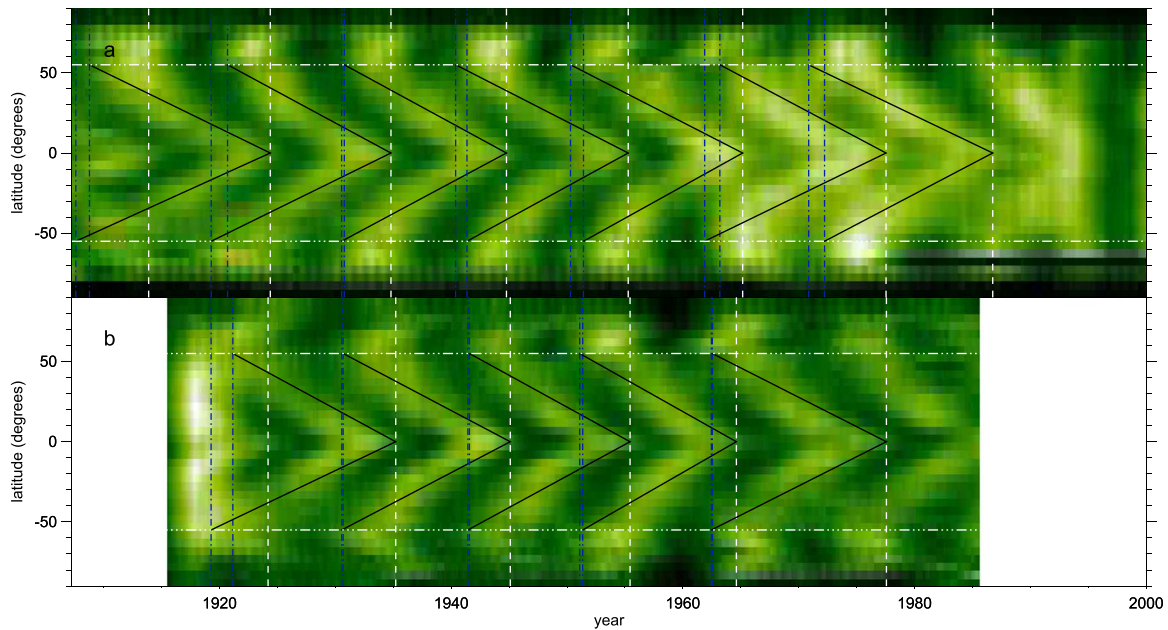


**Figure 3.** Fitted equatorward branches overplotted on smoothed time–latitude plot of NBE density. (a) Fits for KSO NBE time–latitude plot. (b) Fits for MWO NBE time–latitude plot. Data gaps in KSO time–latitude is filled with those from MWO before smoothing. Horizontal white dashed lines depict  $\pm 55^\circ$  latitudes. Vertical blue dashed lines depict the onset of extended equatorward branches and the white vertical dashed lines represent the epoch of equatorward branches reaching the equator, i.e., “Terminators.”

**Table 1**  
Terminator Epochs and Cycle-wise Time-duration of Equatorward Branches

Cycle	Terminators (year)		Duration (years)			
	KSO	MWO	KSO		MWO	
			North	South	North	South
14	1913.88 $\pm$ 0.34					
15	1924.38 $\pm$ 0.54	1924.19 $\pm$ 0.72	15.61 $\pm$ 0.56	16.79 $\pm$ 0.55		
16	1934.80 $\pm$ 0.91	1935.21 $\pm$ 0.74	14.11 $\pm$ 1.11	15.52 $\pm$ 1.30	14.06 $\pm$ 1.95	15.94 $\pm$ 1.88
17	1944.77 $\pm$ 1.47	1945.10 $\pm$ 0.66	14 $\pm$ 1.72	14.23 $\pm$ 1.63	14.43 $\pm$ 1.08	14.55 $\pm$ 1
18	1955.28 $\pm$ 1.17	1955.44 $\pm$ 1.80	14.9 $\pm$ 1.65	13.92 $\pm$ 1.77	13.87 $\pm$ 2.11	14 $\pm$ 2.28
19	1965.16 $\pm$ 2.96	1964.62 $\pm$ 2.12	14.86 $\pm$ 3.91	13.74 $\pm$ 3.23	13.53 $\pm$ 2.37	13.27 $\pm$ 2.53
20	1977.54 $\pm$ 3.57	1977.57 $\pm$ 1.93	14.35 $\pm$ 5.02	15.66 $\pm$ 4.04	15.03 $\pm$ 2.63	
21	1986.75 $\pm$ 3.73		15.89 $\pm$ 4.76	14.52 $\pm$ 4.58		
Mean			14.82 $\pm$ 1.20	14.91 $\pm$ 1.06	14.18 $\pm$ 0.94	14.57 $\pm$ 0.97

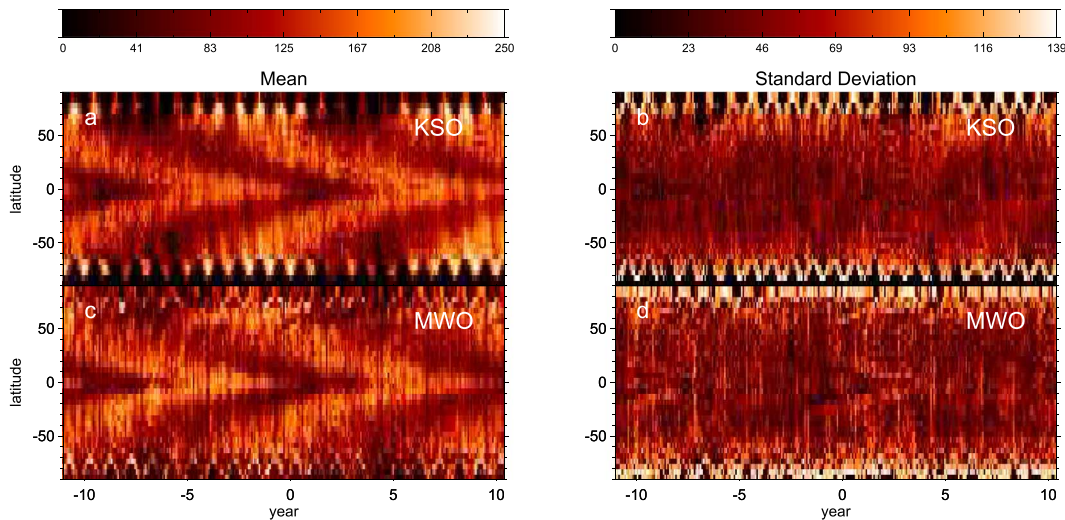


**Figure 4.** Superposed Epoch Analysis on NBE time–latitude distribution. (a) Mean of five epochs defined by  $\pm 11$  yr about terminators for KSO. (b) Standard deviation of five epochs for KSO. (c) Mean of four epochs defined by  $\pm 11$  yr about terminators for MWO. (d) Standard deviation of four epochs for MWO. Figure color scales are put above the top panels tracing the range of statistical moments.

cycles. The standard deviation over five epochs for KSO and four epochs for MWO were calculated to depict the dissimilarity of the cycles (Figures 4(b) and (d)). Within the equatorward branches there is no noticeable variation of standard deviation for both KSO and MWO.

#### 4. Summary and Conclusion

The salient features can be summarized as:

1. Carrington maps from KSO and MWO were processed to automatically detect NBEs for about eight and six solar cycles respectively.
2. Latitudinal density of QS NBEs clearly depicted the signature of ESCs illustrating the coexistence of two equatorward branches for the cycles. Also the time–latitude distribution revealed a close match between MWO and KSO.
3. A latitude  $\approx 55^\circ$  was observed to be the separator between the poleward branch and the equatorward branch.
4. Parameters such as “Terminators” and time duration of equator branches were extracted from the time–latitude distribution of NBEs from both KSO and MWO. Those parameters showed close match within error bars for both the observatories. The equatorward branches were seen to originate at  $\pm 55^\circ$  latitudes every 11 yr taking more than  $\approx 14 \pm 1$  yr to reach the equator.
5. SEA with “Terminators” as key times clearly illustrated the similarity of the ESCs with a considerable match between MWO and KSO.

We should point out that for Cycle-20 onwards, KSO showed higher error bars both in terminator epochs and cycle duration as compared to those from MWO. This might be the effect of poor data density and quality of KSO from cycle-20 that reduced the contrast between equatorward branches after 1965. It should be noted that images of KSO and MWO are not cross-calibrated. For that very reason we treated them separately in this study. Cross-calibration will allow us to fill the gaps in individual Carrington maps and generate even more reliable and consistent results. We wish to pursue that as a future work. For both MWO and KSO least temporal overlap is seen

between equatorward branches of cycle-19 and 20 (Figure 3). In contrast, cycle-19 is observed as the strongest cycle in the last century. Also, previous studies on extended cycles depict a short time difference between sunspot cycle maxima and onset of the extended equatorward branch (McIntosh et al. 2014). This gives an indication that magnetic interaction between the two equatorward bands might modulate sunspot cycle amplitude to a certain extent based on the duration of temporal overlap and may also contribute in the decay rate of the sunspot cycle.

Thus our findings from the Ca II K historical data sets are on par with the results on ESCs from space-based data and coronal green line observations. We could validate those results for several cycles starting from cycle 15. Thus, this study established the fact that NBEs detected from chromospheric networks are effective proxies for ESCs. Such a consistent observation of an overlapping cycle may provide valuable inputs to traditional dynamo models. Coexistence of two equatorward branches and their magnetic interaction can play a role in better prediction of sunspot cycles as well space weather with a possible impact on Earth’s climate (McIntosh et al. 2015; Dikpati et al. 2019).

We would like to thank all of the observers at Kodaikanal for their contributions to build this enormous resource over the last 100 yr. KSO data is now available for public use at <http://kso.iiap.res.in/data>. We also thank the Science & Engineering Research Board (SERB) for the project grant (EMR/2014/000626). We would also like to acknowledge the IUSSTF/JC-011/2016 project grant for supporting this work. We are grateful to the team members of the project on Reconstructing Solar and Heliospheric Magnetic Field Evolution Over the Past Century supported by the International Space Science Institute (ISSI), Bern, Switzerland for giving important suggestions to this project.

#### ORCID iDs

Subhamoy Chatterjee  <https://orcid.org/0000-0002-5014-7022>

Dipankar Banerjee  <https://orcid.org/0000-0003-4653-6823>

Scott W. McIntosh  <https://orcid.org/0000-0002-7369-1776>  
 Mausumi Dikpati  <https://orcid.org/0000-0002-2227-0488>

### References

- Altrock, R. C. 1997, *SoPh*, **170**, 411  
 Chatterjee, S., Banerjee, D., & Ravindra, B. 2016, *ApJ*, **827**, 87  
 Chatterjee, S., Mandal, S., & Banerjee, D. 2017, *ApJ*, **841**, 70  
 Chree, C. 1913, *RSPTA*, **212**, 75  
 Dikpati, M., McIntosh, S. W., Chatterjee, S., et al. 2019, *NatSR*, **9**, 2035  
 Howe, R. 2009, *LRSP*, **6**, 1  
 Juckett, D. A. 1998, *SoPh*, **183**, 201  
 Labonte, B. J., & Howard, R. 1982, *SoPh*, **75**, 161  
 McIntosh, S. W., Leamon, R. J., Dikpati, M., Fan, Y., & Rempel, M. 2019, arXiv:1901.09083  
 McIntosh, S. W., Leamon, R. J., Hock, R. A., Rast, M. P., & Ulrich, R. K. 2011, *ApJL*, **730**, L3  
 McIntosh, S. W., Leamon, R. J., Krista, L. D., et al. 2015, *NatCo*, **6**, 6491  
 McIntosh, S. W., Wang, X., Leamon, R. J., et al. 2014, *ApJ*, **792**, 12  
 Priyal, M., Banerjee, D., Karak, B. B., et al. 2014, *ApJL*, **793**, L4  
 Robbrecht, E., Wang, Y.-M., Sheeley, N. R., Jr., & Rich, N. B. 2010, *ApJ*, **716**, 693  
 Sheeley, N. R., Jr., Cooper, T. J., & Anderson, J. R. L. 2011, *ApJ*, **730**, 51  
 Snodgrass, H. B., & Wilson, P. R. 1987, *Natur*, **328**, 696  
 Song, W., Feng, X., & Hu, Y. 2007, *ApJL*, **667**, L101  
 Tappin, S. J., & Altrock, R. C. 2013, *SoPh*, **282**, 249  
 Tlatov, A. G. 2007, *AN*, **328**, 1027  
 Tlatov, A. G., Vasil'eva, V. V., & Pevtsov, A. A. 2010, *ApJ*, **717**, 357  
 Wilson, P. R., Altrocki, R. C., Harvey, K. L., Martin, S. F., & Snodgrass, H. B. 1988, *Natur*, **333**, 748